Co-continuous Metal-Ceramic Nanocomposites

Xiao Feng Zhang[1*], Gabriel Harley[1,2], Lutgard C. De Jonghe[1,2]

[1] *Materials Sciences Division, Lawrence Berkeley National Laboratory, University of California, Berkeley, CA 94720*

[2] *Department of Materials Science & Engineering, University of California, Berkeley, CA 94720*

ABSTRACT

A room temperature technique was developed to produce continuous metal nanowires embedded in random nanoporous ceramic skeletons. The synthesis involves preparation of uniform, nanoporous ceramic preforms, and subsequent electrochemical metal infiltration at room temperature, so to avoid materials incompatibilities frequently encountered in traditional high temperature liquid metal infiltration. Structure and preliminary evaluations of mechanical and electronic properties of copper/alumina nanocomposites are reported.

Keywords: Metal/ceramic nanocomposite, Cu, porous Al_2O_3, electrochemical infiltration.

[*]Corresponding author. Email: xfzhang@lbl.gov

Nanograin ceramics have been reported to exhibit dramatically increased strength, hardness, and superplasticity.[1] Similarly, metallic nanowires can have unusual physical properties, such as quantized electron, photon, and phonon transport.[2-6] Enhanced strength, plasticity, and hardness were also observed for nanocrystalline metals as a result of limited dislocation mobility[1,7-11]. While other deformation mechanisms, such as desclination activity[12] may participate at high deformation rates, diffusion-controlled grain boundary sliding[13-15] is likely to be the dominant deformation mechanism for nanosized grain materials. It was also reported that scale effects are significant factors in determining strength and plasticity of metals, alloys, and superalloys for sizes up to as much as several micrometers.[16] When co-continuous metal/ceramic composites are created in which both the metallic and the ceramic components are of nanoscale size, the nature of the high interface/volume ratio and synergy of the combined physical properties may lead to a novel class of structural or functional materials.

To avoid materials incompatibilities associated with the elevated temperatures required for molten metal infiltration, room temperature electrochemical infiltration of porous ceramic preforms has been considered.[17-18] Most published results have been for metal electrochemical infiltration of either submicron porous matrices[18] or micrometer thin anodized Al_2O_3 membranes with one-dimensional nanopore channels .[6,17,19-20] The present paper describes a method in which a nanograin ceramic compact is first produced with homogeneous nanoporosity, and subsequently filled with a continuous metallic nanowire network by room temperature electrochemical infiltration.

Nanoporous alumina matrices (10 mm diameter and 1 mm thick, 40% porosity) were made by compacting and free sintering 20 nm γ-Al_2O_3 nanopowder. The samples were placed in a holder, and electrochemical infiltration of Cu into the interconnected nanopore channels was done in a 0.2M $CuSO_4$ + 2M H_2SO_4 + deionized water electroplating bath, with a Cu anode and the sample/Cu cathode 1.5 cm apart. Optimization of combined d.c. and a.c. currents was essential for efficient infiltration. The infiltrated samples were dried, and post-annealed at 500^{o}C in a He/4% H_2 atmosphere. The structure of

the Cu/Al_2O_3 nanocomposites was studied using X-ray diffraction (XRD), scanning electron microscopy (SEM), and transmission electron microscopy (TEM). Experimental details about processing of Al_2O_3 nanoporous preforms, electrochemical Cu infiltration, and structural characterization instruments can be found with supporting information.

Figure 1a and 1b show an SEM micrograph and corresponding XRD for an as-pressed γ-Al_2O_3 compact, while Figure 1c and 1d show a sintered, nanoporous α-Al_2O_3 compact (58% dense) and corresponding XRD. Complete γ-to-α transformation of the alumina took place during heating to 1100^{o}C and holding for less than 0.5 hr, in agreement with other sintering studies on the same type of powders.[21] The particle agglomerate size in the green body ranges from 10 to 40 nm while after sintering the grain diameters coarsened to 80±20 nm. Interconnected pore channels with diameters of 10 to 70 nm were distributed homogeneously through the sintered compacts. BET (Brunauer-Emmett-Teller) analysis further demonstrated that 90% of the pore channels had diameters ranging between 20 and 65 nm, at a specific internal surface area of 13.6±0.1 m^2/g.

After Cu infiltration, the color of the Al_2O_3 matrices changed from white to dark brown. Because XRD revealed the pure α-Al_2O_3 phase and face-centered cubic Cu structure, the dark brown color is due to the nanoscale dimensions of the Cu.[22] Copper oxide reflections were absent in the XRD.

SEM and TEM examinations confirmed that Cu nanowires were formed inside the pore channels. A typical morphology for the Cu/Al_2O_3 nanocomposites is shown in Figure 2a, in which dark and gray image contrasts are for Cu wires and Al_2O_3 grains, respectively. Uniform Cu nanowire networks are embedded in the nanopores, with discrete interfaces between the Cu and the Al_2O_3, free of secondary phases, as confirmed by high-resolution TEM, Figure 2b, and by electron nanoprobe chemical analysis. Statistical measurements yielded a mean diameter of 30±9 nm for the Cu nanowires. Twinning in the Cu nanowires was often observed, and some twining grains extended as far as 0.9 μm through the Cu network, indicating that the Cu nanowires can be single crystalline on a length scale of close to a micron, spanning several interconnected pore channels.

Preliminary electrical property tests showed that at room temperature, the electrical resistivity throughout the 1 mm thickness of the samples was on the order of 10^{-6} Ωm, confirming the continuity of the Cu nanowire network. Resistivity measurements were also conducted at up to 400°C in air. Significant departure from the low resistivity regime, due to copper oxidation, was not apparent below 150°C.

Vickers indentation was performed on polished surfaces of nanoporous Al_2O_3 pellets and Cu/Al_2O_3 nanocomposites, respectively. Figure 3 shows diamond shaped indents made with 1 kg load. The much shorter diagonal length for the composite indicates enhanced resistance to deformation compared with pure porous Al_2O_3. This is attributed to the Cu nanowire network that provides structural support for the alumina skeleton. The Vickers hardness is measured to be 7.3±0.6 GPa for the nanocomposites, about twice as high as that for the nanoporous Al_2O_3 matrices (3.8±0.1 GPa); the latter is consistent with the value derived from the hardness dependence equation for porous ceramics.[23] Some evidences of potential toughening mechanisms, such as crack deflection by Cu nanowires, metal phase ductility, and crack tip blunting were also found by TEM, as shown in Figure 4.

The significance of the processing technique developed here is that the distribution, size, and connectivity of the nanowire phase may be widely varied by choice of ceramic particle size and sintering conditions. An opportunity is thus provided for the design of a variety of nanoscale structures with potential applications in MEMS, and other micromechanical or functional micro- and nano-devices.

In conclusion, Cu/Al_2O_3 random, co-continuous nanocomposites consisting of Cu nanowire/nanograin Al_2O_3 were produced at room temperature by electrochemical Cu infiltration of homogeneous, nanoporous alumina preforms. The 40% porosity Al_2O_3 preforms are composed of 80 nm α-Al_2O_3 skeleton grains with ~40 nm diameter interconnected pores. The filling of the pore channels formed uniformly distributed, three-dimensional Cu nanowire networks embedded in the nanograin Al_2O_3 skeletons. The nanocomposites are electrical conductive, and hardness is doubled compared with the unfilled nanoporous alumina.

Acknowledgment. This work was supported by the Director, Office of Science, Office of Basic Energy Sciences, Division of Materials Sciences and Engineering of the U.S. Department of Energy under Contract No. DE-AC03-76SF0098. Part of this work was made possible through the use of the National Center for Electron Microscopy facility at the Lawrence Berkeley National Laboratory. We thank Man I Lei, Rong Yu, and Paul Dearhouse for technical assistance.

Supporting Information Available: Experimental details describing processing of Al_2O_3 nanoporous preforms, electrochemical Cu infiltration, and structural characterization instruments. This material is available free of charge via the Internet at http://pubs.acs.org.

Figure Captions

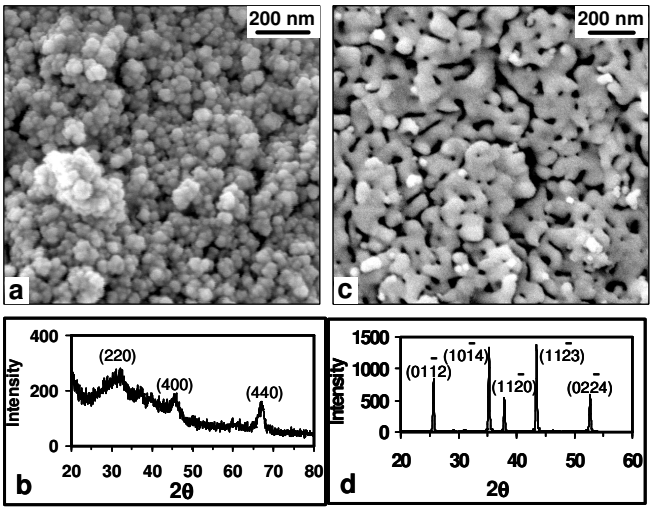

Figure 1. (a) SEM image for γ-Al_2O_3 nanopowder compact. Spherical nanoparticles can be seen. (b) XRD for the as-pressed compact after heating at 800°C for 24 hrs. The peak indices are consistent with the γ-Al_2O_3 phase. The broadening of the XRD peaks is indicative of nanoparticles. (c) SEM image taken from a fractured surface of a sintered compact. Al_2O_3 nanograins and interconnected nanopore channels are observed. (d) XRD for a compact sintered at 1100°C. The peak indices agree with the α-Al_2O_3 phase.

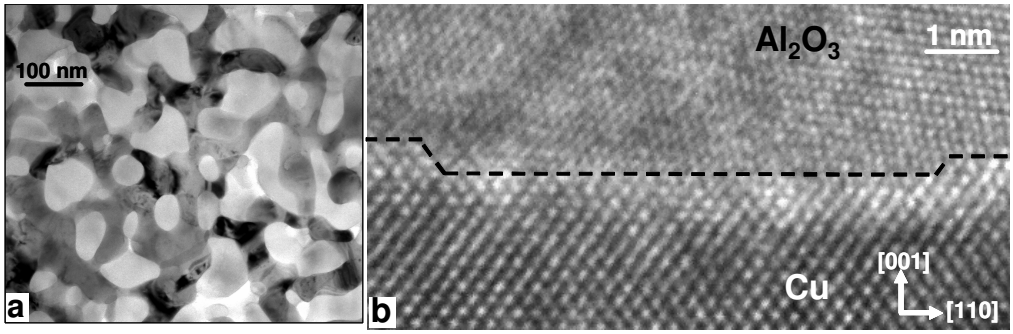

Figure 2. (a) TEM bright-field image showing microstructure of a Cu/Al_2O_3 nanocomposite. The Al_2O_3 nanograins appear gray, and the Cu nanowires appear dark. A uniformly distributed Cu nanowire network is evident. (b) High-resolution TEM image showing a Cu/Al_2O_3 interface (marked by a dashed line). The interface is smooth at the atomic level, and free of secondary phases.

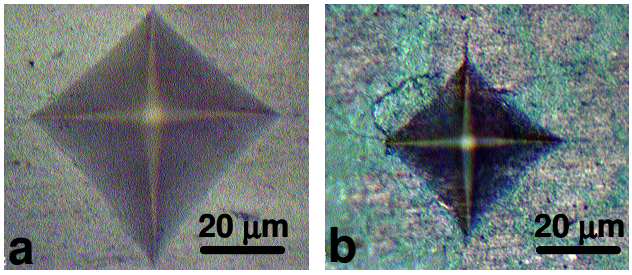

Figure 3. Vickers indents on (a) a nanoporous Al_2O_3 compact, and (b) a Cu/Al_2O_3 nanocomposite. The much shorter diagonal length in (b) corresponds to a remarkably enhanced deformation resistance of the nanocomposites compared with Al_2O_3 matrices.

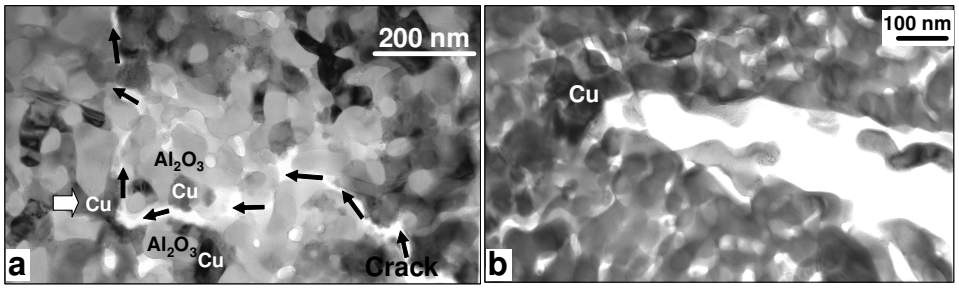

Figure 4. TEM images of (a) Crack propagation through the nanocomposite, along Al_2O_3/Al_2O_3 and Cu/Al_2O_3 interfaces. Note the strong crack deflection at the arrowed Cu ligament. (b) Crack tip blunting at Cu ligament.

References

(1) Weertman, J.R.; Farkas, D.; Hemker, K.; Kung, H.; Mayo, M.; Mitra, R.; Van Swygenhoven, H. *MRS Bulletin* **1999**, 24, 44-50.

(2) Muller, C.J.; van Ruitenbeek, J.M.; de Jongh, L. J. *Phys. Rev. Lett.* **1992**, 69, 140-143.

(3) Van Houten, H.; Beenakker, C.W.J. *Physics Today* **1996,** 7, 22-27.

(4) Kouwenhoven, L.P.; Venema, L.C. *Nature* **2000**, 404, 943-944.

(5) Schwab, K.; Henriksen, E.A.; Worlock, J.M.; Roukes, M.L. *Nature* **2000**, 404, 974-977.

(6) Zhang, Z.; Sun, X.; Dresselhaus, M.S.; Ying, J.Y.; Heremans, J. *Phys. Rev. B* **2000**, 61, 4850-4861.

(7) Nieh, T.G.; Wadsworth, J. *Scripta Metall. Mater.* **1991**, 25, 955-958.

(8) Sanders, P.G.; Eastman, J.A.; Weertman, J.R. *Acta Mater.* **1997**, 45, 4019-4025.

(9) Yip, S. *Nature* **1998**, 391, 532-533.

(10) McFadden, S.X.; Mishra, R.S.; Valiev, R.Z.; Zhilyaev, A.P.; Mukherjee, A.K. *Nature* **1999**, 398, 684-686.

(11) Lu, L.; Sui, M.L.; Lu, K. *Science* **2000**, 287, 1463-1466.

(12) Murayama, M.; Howe, J.M.; Hidaka, H.; Takaki, S. *Science* **2002**, 295, 2433-2435.

(13) Van Swygenhoven, H.; Derlet, P.M. *Phys. Rev. B* **2001**, 64, 224105-224109.

(14) Van Swygenhoven, H. *Science* **2002**, 296, 66-67.

(15) Schiøtz, J.; Jacobsen, K.W. *Science* **2003**, 301, 1357-1359.

(16) Uchic, M.D.; Dimiduk, D.M.; Florando, J.N.; Nix, W.D. *Science* **2004**, 305, 986-989.

(17) Searson, P.C. *Solar Energy Materials and Solar Cells* **1992**, 27, 377-388.

(18) Hirata, Y.; Kyoda, K.; Hatano, H. *Mat. Lett.* **1994**, 21, 155-159.

(19) Saito, M.; Kirihara, M.; Taniguchi, T.; Miyagi, M. *Appl. Phys. Lett.* **1989**, 55, 607-609.

(20) Yin, A.J.; Li, J.; Jian, W.; Bennett, A.J.; Xu, J.M. *Appl. Phys. Lett.* **2001**, 79, 1039-1041.

(21) Ahn, J-P.; Park, J-K.; Lee, H.-W. *NanoStructured Materials*, **1999,** 11, 133-140.

(22) Liz-Marzan, L.M. *Materials today* **2004**, 2, 26-31.

(23) McColm, I.J. *Ceramic Hardness*, Plenum Press: New York, 1990; p 8.